12-15-2019

Regional gene repression by DNA double-strand breaks in G1 phase cells

Caitlin E. Purman

Patrick L. Collins

Sofia I. Porter

Ankita Saini

Harshath Gupta

See next page for additional authors

Authors

Caitlin E. Purman, Patrick L. Collins, Sofia I. Porter, Ankita Saini, Harshath Gupta, Barry P. Sleckman, and Eugene M. Oltz

AMERICAN SOCIETY FOR MICROBIOLOGY | Molecular and Cellular Biology®

RESEARCH ARTICLE

Regional Gene Repression by DNA Double-Strand Breaks in G_1 Phase Cells

Caitlin E. Purman,[a,b] Patrick L. Collins,[a,d] Sofia I. Porter,[a,d] Ankita Saini,[a,d] Harshath Gupta,[a] Barry P. Sleckman,[c] Eugene M. Oltz[a,d]

[a]Department of Pathology and Immunology, Washington University School of Medicine, St. Louis, Missouri, USA
[b]Molecular Genetic and Genomics Graduate Program, Washington University School of Medicine, St. Louis, Missouri, USA
[c]Department of Pathology and Laboratory Medicine, Weill Cornell Medical College, New York, New York, USA
[d]Department of Microbial Infection and Immunity, The Ohio State University, Columbus, Ohio, USA

ABSTRACT DNA damage responses (DDR) to double-strand breaks (DSBs) alter cellular transcription programs at the genome-wide level. Through processes that are less well understood, DSBs also alter transcriptional responses locally, which may be important for efficient DSB repair. Here, we developed an approach to elucidate the *cis*-acting responses to DSBs in G_1 phase cells. We found that DSBs within a gene body silence its expression, as well as the transcription of local undamaged genes at a distance defined by the spread of γ-H2AX from the DSB. Importantly, DSBs not only repress ongoing transcription but also block the inducible expression of regional genes. DSB-mediated transcriptional repression depends on DDR signaling but does not require the generation of inaccessible chromatin. Our findings demonstrate that in G_1 phase cells, DDR signaling establishes a robust and extensive region of transcriptional repression spreading from DSB sites and introduce an approach to study the mechanistic impact of targeted DNA breaks in nearly any chromatin environment.

KEYWORDS DNA damage, DNA damage signaling, chromatin, nonhomologous DNA end joining, transcriptional regulation

DNA double-strand breaks (DSBs) are dangerous genomic lesions that derive from a variety of sources, including exogenous agents (e.g., ionizing radiation), basic cellular processes (e.g., transcription and DNA replication), or developmental programs (e.g., antigen receptor gene rearrangement) (1–3). The consequences of aberrant DSB repair range from apoptosis to mutations that fuel carcinogenesis. To protect against these adverse outcomes, eukaryotic cells have developed two major pathways for DSB repair: nonhomologous end joining (NHEJ) and homologous recombination (HR). NHEJ occurs throughout the cell cycle and involves the direct ligation of broken DNA ends, whereas HR, which uses the sister chromatid as a template for repair, is restricted primarily to the S and G_2 phases (4, 5). Given that most mammalian somatic cells reside in G_0/G_1, NHEJ represents the major pathway for DSB repair and genome maintenance. However, NHEJ-mediated repair also can lead to chromosomal rearrangements, especially in the context of complex DSB end structures or chromatin environments in which breaks are not resolved quickly (6–8). As such, a critical goal is to understand the interplay between the genetic, epigenetic, and structural features of a chromosomal break site, as well as the downstream functional outcomes in G_0/G_1 phase cells.

DSBs initiate a canonical DNA damage response (DDR) that regulates not only their repair but also other cellular processes, including cell cycle arrest, transcriptional programs, and chromatin reorganization (3, 9–11). In G_0/G_1 phases, DSBs are sensed by the Mre11/Rad50/Nbs1 (MRN) complex and the Ku70/80 heterodimer, which activate

Citation Purman CE, Collins PL, Porter SI, Saini A, Gupta H, Sleckman BP, Oltz EM. 2019. Regional gene repression by DNA double-strand breaks in G_1 phase cells. Mol Cell Biol 39:e00181-19. https://doi.org/10.1128/MCB.00181-19.

Address correspondence to Barry P. Sleckman, bas2022@med.cornell.edu, or Eugene M. Oltz, eugene.oltz@osumc.edu.

Received 21 April 2019
Returned for modification 19 May 2019
Accepted 24 September 2019
Accepted manuscript posted online 7 October 2019
Published 25 November 2019

the phosphatidylinositol 3-kinase-like protein kinase (PI3KK) family members ATM and DNA-PKcs. These kinases phosphorylate hundreds of downstream effector molecules that function in the canonical DDR (12–14). A key target of ATM and DNA-PKcs is the histone variant H2AX, which is phosphorylated on serine 139, forming γ-H2AX. This histone posttranslational modification can propagate from the break site, extending for megabases along chromatin to form γ-H2AX domains (15). The γ-H2AX domains act as scaffolds for recruitment and retention of other nuclear factors involved in histone modification, chromatin remodeling, end processing, and repair (16, 17). Thus, DSBs initiate a signaling cascade that drives substantial alterations in the genomic microenvironment, including the regional landscape of chromatin and nuclear factors. To this end, the downstream functional consequences of DSB signaling on local, regional, and global gene expression in G_0/G_1 phase cells remain largely unexplored.

In cycling cells, DSBs at or near an active gene transiently repress its transcription via ATM- and DNA-PKcs-dependent mechanisms (18–22). However, DSBs activate divergent signaling pathways, depending on the cell cycle phase in which they occur, leading to vastly different cellular responses. For example, DDR signaling activates distinct checkpoint and repair pathways in G_1 versus S versus G_2 phases, each of which recruits its own sets of factors to DSB-proximal chromatin (23, 24). As such, the specific cell cycle phase in which a DSB occurs may differentially impact local chromatin reorganization, DSB end processing, and, likely, the transcription of genes near a lesion. With regard to the transcription of genes near a lesion, a persistence of transcription near a break site could cooperate or interfere with repair processes, especially given that NHEJ factors form complexes with RNA polymerase II (RNAPII) when DSBs occur in transcribed genes (25). RNA-DNA hybrids also accumulate at endogenous DSBs in transcriptionally active regions, where they may influence NHEJ and HR (26, 27). Conversely, RNA polymerase complexes and RNA-DNA hybrid structures at the DSB site could act as physical barriers to end processing and repair (28, 29). Thus, controlling transcriptional activity in the vicinity of a DSB may be a critical component of the mechanisms that facilitate the rapid and precise resolution of the lesion (29, 30).

We developed an approach to study DDR regulation of transcription at loci harboring a single, targeted DSB in G_0/G_1 phase cells. We chose a cell system in which DSBs persist unrepaired, which generates a sustained DNA damage response and which allows us to detect changes that may otherwise be obscured by rapid repair. We found that DSBs targeted to sites either within or several kilobases outside of a gene body repress its ongoing transcription. Importantly, the same lesions also block induced expression of the proximal gene, indicating that ongoing transcription is not required for DSB-mediated repression. Remarkably, we found that transcriptional repression spreads to distal genes within the γ-H2AX domain in a DDR-dependent manner. Together, our findings provide a rigorous demonstration that genomic DSBs incurred in G_0/G_1 suppress regional gene expression and underscore the utility of our experimental model for a systematic dissection of the responses to DSBs within a range of chromatin environments.

RESULTS

Generation of persistent, targeted DSBs in G_1 phase cells. To interrogate the local transcriptional response to DSBs, we developed an experimental system to generate high levels of persistent DSBs at predetermined sites in the genome of G_1-synchronized cells (Fig. 1A). Specifically, we employed a v-Abl-transformed murine pre-B cell line (Abelson line) that can be arrested in G_1 phase by treatment with the Abl kinase inhibitor imatinib (STI571 or STI) (31). We chose a cell line that was deficient for the core NHEJ factor, DNA ligase IV. Because NHEJ is the major DSB repair pathway utilized in noncycling cells, DSBs persist unrepaired in these Abelson lines when they are placed under G_1 arrest (32).

To target DSBs at preselected genomic sites, a doxycycline-inducible Cas9 (pCW-Cas9) was stably integrated into Abelson cells deficient for DNA ligase IV (*LigIV*$^{-/-}$*:iCas9* cells). Treatment of cycling *LigIV*$^{-/-}$*:iCas9* cells with doxycycline induced robust Cas9

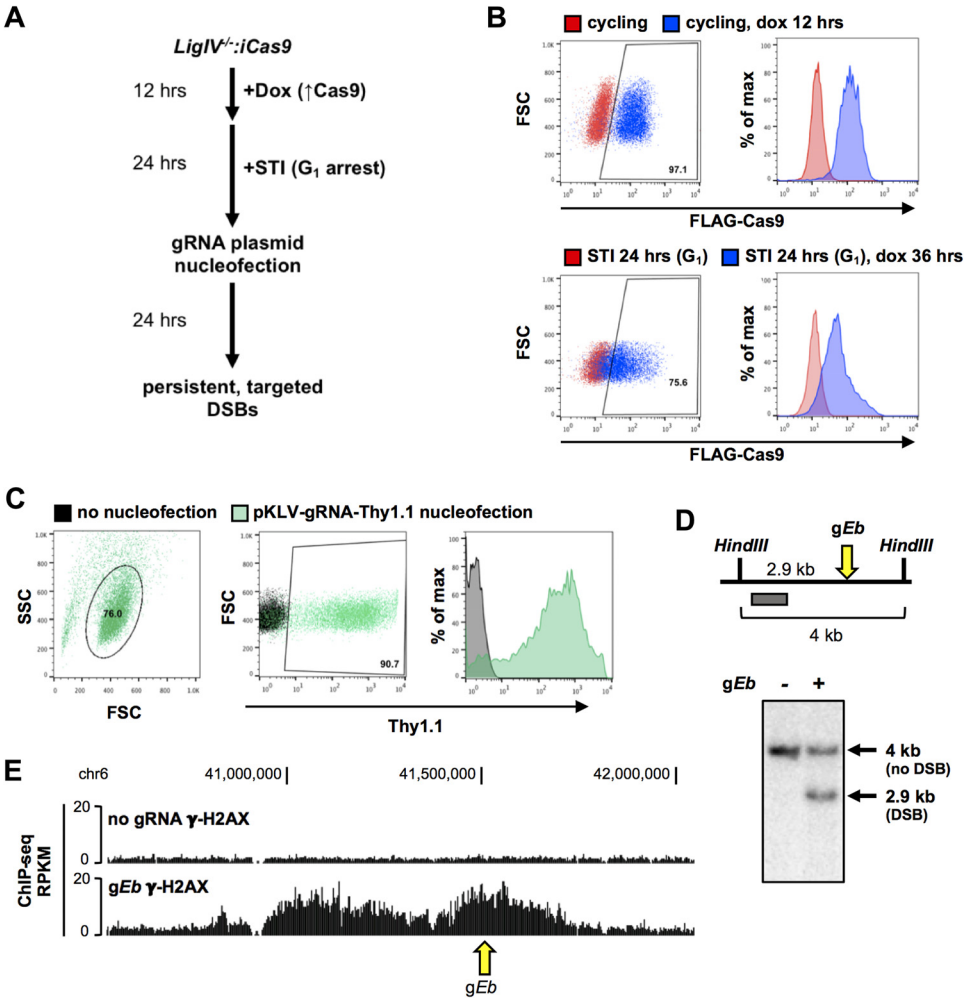

FIG 1 Generation of persistent, targeted breaks in G_1 phase cells using CRISPR/Cas9. (A) Work flow for CRISPR/Cas9-induced breaks in *LigIV*$^{-/-}$*:iCas9* v-Abl-transformed pre-B cells. (B) Intracellular staining and flow cytometric analysis for FLAG-Cas9 in cycling (top) and G_1-arrested (bottom) *LigIV*$^{-/-}$*:iCas9* cells that were untreated or treated with doxycycline for the indicated times. (C) Staining for the Thy1.1 cell surface marker and flow cytometric analysis for Thy1.1 in G_1-arrested *LigIV*$^{-/-}$*:iCas9* cells nucleofected with the pKLV-U6gRNA(BbsI)-UbcThy1.1 gRNA expression vector and nonnucleofected cells. (D) (Top) Schematic of the Southern blotting strategy to detect cleaved alleles at the enhancer of *Tcrb* (*Eb*). (Bottom) Southern blot showing intact and cut *Eb* alleles at 0 and 24 h after nucleofection of *LigIV*$^{-/-}$*:iCas9* cells with a gRNA plasmid targeting *Eb* (g*Eb*). (E) UCSC Genome Browser screenshot depicting the γ-H2AX ChIP-seq signal at the *Eb* locus in G_1-arrested, *LigIV*$^{-/-}$*:iCas9* cells at 24 h after nucleofection with g*Eb* (bottom track) or no gRNA (top track). The arrow indicates the g*Eb* target site. Dox and dox, doxycycline; SSC, side scatter; FSC, forward scatter.

protein expression, which persisted after G_1 arrest (Fig. 1B). Sequences corresponding to several genomic sites were cloned into a modified pKLV-gRNA plasmid that contained a guide RNA (gRNA) expression cassette and that harbored the Thy1.1 cell surface marker. Nucleofection of the gRNA plasmid into G_1-arrested *LigIV*$^{-/-}$*:iCas9* cells resulted in >90% Thy1.1 positivity (Fig. 1C). G_1-arrested cells treated with doxycycline and transfected using nucleofection (nucleofected) with a gRNA expression vector designed to target the endogenous enhancer of *Tcrb* (g*Eb*) accumulated breaks at the *Eb* target site (Fig. 1D). To ensure that Cas9-generated DSBs elicit a canonical DNA damage response (DDR) in our system, we mapped γ-H2AX formation in cells nucleofected with g*Eb* or no gRNA as a control. Consistent with the findings of prior studies, the γ-H2AX modification extended for several hundred kilobases on either side of the break site in cells nucleofected with g*Eb* (Fig. 1E). No γ-H2AX domain was observed in the control cells or at other loci in g*Eb*-expressing cells (Fig. 1E; data not shown). These

data indicate that DDR signaling is intact in these G_1-arrested cells and is specific to regions targeted for a DSB.

Persistent DSBs in G_1 phase repress transcription of an active endogenous gene. We first set out to determine how persistent DSBs within an active endogenous gene affect its transcription. We chose to target the *Irf4* locus, which is constitutively expressed in our cell line. G_1-arrested, *LigIV*$^{-/-}$*:iCas9* cells were nucleofected with a gRNA targeting a site within *Irf4* intron 6, about 6.3 kb downstream of the *Irf4* promoter (Fig. 2A). As expected, we observed high levels of persistent DSBs at the target site at 24 h postnucleofection (Fig. 2B). A persistent break within the *Irf4* gene body significantly reduced the levels of its corresponding mRNA, as measured by reverse transcription (RT)-quantitative PCR (qPCR) analysis at 24 h postnucleofection (Fig. 2C). In contrast, expression of a control gene, *Tnks2*, located on a different chromosome, was unaffected (Fig. 2C). Analysis of nascent transcript levels yielded comparable results (Fig. 2D). Similar reductions in transcript levels were observed using primers for regions upstream (primer set P1) or downstream (primer set P2) of the DSB site. Because the break interrupts the transcriptional unit, the observed effects on transcription could be due to active repression, the instability of truncated transcripts, or both. To determine whether DSB repression of transcription requires the disruption of the gene body, we targeted Cas9 to a site 9.5 kb upstream of the *Irf4* promoter (Fig. 2A and E). As observed for breaks within the gene body, a DSB upstream of the same transcriptional unit led to a nearly identical reduction in total and nascent transcripts (Fig. 2F and G). We conclude that single DSBs in G_1 phase can silence expression of proximal genes, even when they do not directly interrupt the transcriptional unit.

DSBs block transcriptional activation of an inducible endogenous gene. To understand whether DSBs can regulate the induction of gene expression, we targeted Cas9 to the endogenous *Ifit* locus, which harbors a cluster of interferon-inducible genes. Importantly, regulation of these genes is restricted to the activities of their proximal promoters, which harbor multiple interferon-stimulated response elements (ISREs) that bind the STAT1/2 transcription factors (33, 34). Indeed, expression of *Ifit1* is rapidly induced in G_1-arrested, *LigIV*$^{-/-}$ Abelson cells upon treatment with the type I interferon, interferon beta (IFN-β) (Fig. 3A), without inducing a DNA damage response (Fig. 3B). Thus, the *Ifit1* locus provides an excellent model to test if DSBs not only silence ongoing gene transcription but also block the activation of transcription at genes proximal to the lesion.

We targeted Cas9 to two sites at the *Ifit1* locus, one 3 kb downstream of *Ifit1* (g*Ifit1* 3′) and one within the *Ifit1* gene body (g*Ifit1* intron) (Fig. 3C to E). The former DSB lies ~12 kb 3′ of the *Ifit1* promoter, while the latter is in the single *Ifit1* intron, ~6.6 kb 3′ to the promoter (Fig. 3C). To test whether each DSB affected ongoing transcription, we induced *Ifit1* expression 2 h prior to nucleofection with gRNAs (Fig. 3F). We then assessed nascent transcript levels at 24 h postnucleofection using primer sets upstream (primer set P1) and downstream (primer set P3) of the intronic break site, as well as spliced *Ifit1* transcripts (primer set P2) (Fig. 3C). As expected, nascent mRNA levels were reduced when a DSB was introduced into the *Ifit1* intron, which disrupts the transcriptional unit (Fig. 3G). Importantly, repression also was observed upon introduction of the g*Ifit1* 3′ DSB downstream of the transcriptional unit and its polyadenylation site (Fig. 3H). As a control for general effects on the interferon response, we found that transcript levels for *Isg15*, an IFN-β-induced gene on chromosome 4, were unaltered (Fig. 3G and H). Consistent with our data for *Irf4*, we conclude that a DSB either within or outside the *Ifit1* gene represses its ongoing transcriptional activity.

Notably, the *Ifit1* locus also allowed us to gauge the impact of a DSB on induced transcription rather than simply ongoing gene expression. For this purpose, we treated the G_1-arrested cells with IFN-β at 24 h after nucleofection, the time point of maximal DSB accumulation (Fig. 3D, E, and I). Analysis of the induced mRNA levels after 4 h of IFN-β treatment revealed a DSB-dependent reduction in *Ifit1* transcripts, regardless of whether the DSB was targeted within or downstream of the *Ifit1* gene body (Fig. 3J and

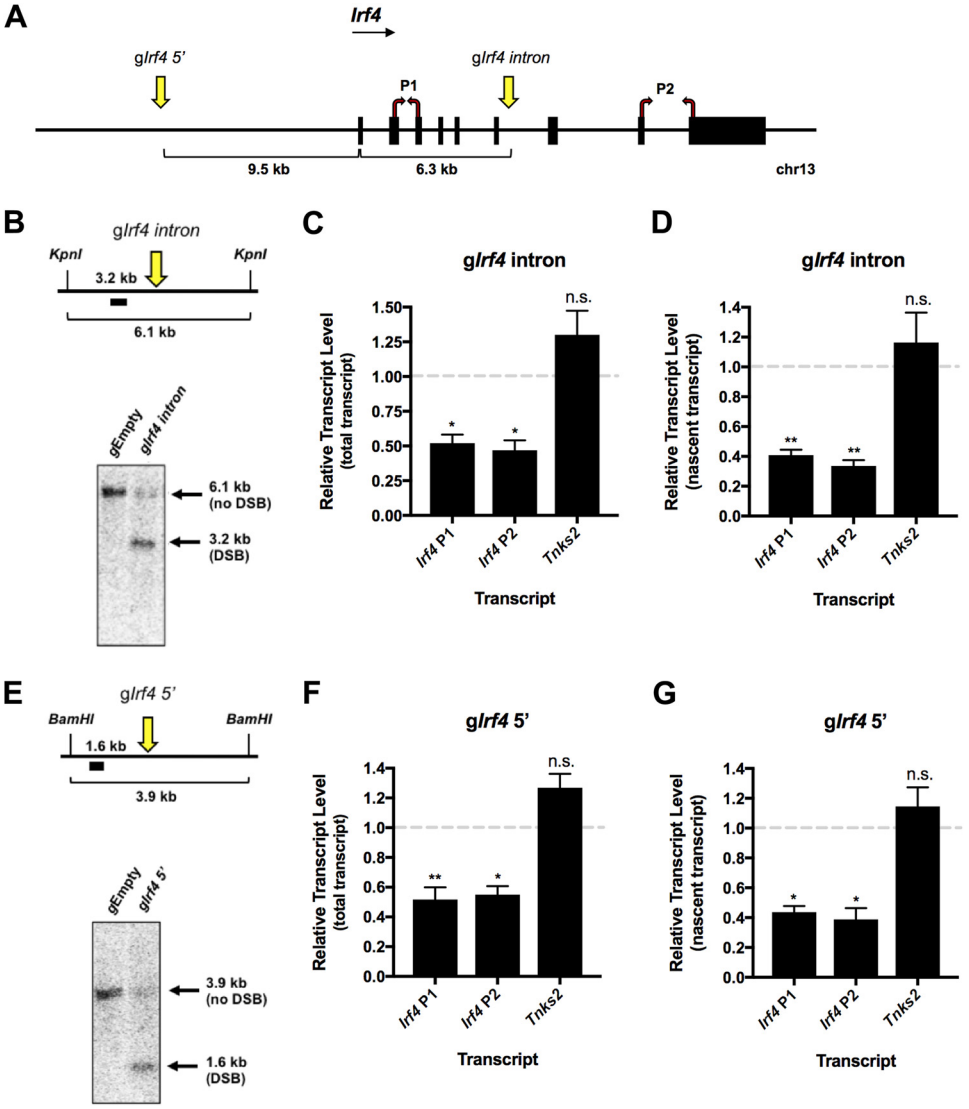

FIG 2 Gene body or 5′ DSBs attenuate expression of the endogenous *Irf4* gene. (A) Schematic of the *Irf4* locus. gRNA target sites are denoted by yellow arrows. The qPCR primers used to detect *Irf4* transcripts are shown as red arrows. The distances between gRNA target sites and the *Irf4* promoter are indicated. chr13, chromosome 13. (B) Schematic of the Southern blotting strategy for detecting cleaved alleles at the *Irf4* intronic gRNA target site (g*Irf4* intron) (top) and Southern blot showing intact and cut *Irf4* alleles 24 h after nucleofection of doxycycline-treated, G_1-arrested *LigIV*$^{-/-}$*:iCas9* cells with the empty gRNA vector or g*Irf4* intron (bottom). (C) RT-qPCR analysis of total *Irf4* transcript levels (primer pairs P1 and P2) and a control gene, *Tnks2*, at 24 h after nucleofection with a gRNA targeting *Irf4* intron 6 (g*Irf4* intron). The transcript levels relative to those in cells nucleofected with an empty gRNA control vector (gEmpty) are shown. (D) RT-qPCR analysis of nascent transcript levels from samples for which the results are shown in panel C, performed using the Click-iT nascent RNA capture technology. Cells were pulsed with 5-ethynyl uridine (EU) 1 h prior to harvesting for RNA isolation. (E) Southern blot schematic and Southern blot, as described in the legend to panel B, for gRNA targeting the region 9.5 kb upstream of the *Irf4* promoter (g*Irf4* 5′). (F) RT-qPCR analysis of total transcript levels, as described in the legend to panel C, for cells nucleofected with a gRNA targeting the region 9.5 kb upstream of the *Irf4* promoter (g*Irf4* 5′). (G) RT-qPCR analysis of nascent transcript levels, as described in the legend to panel D, from samples for which the results are shown in panel F. Data from panels C and D and from panels F and G represent those from 3 independent experiments ($n = 3$). Error bars show the SEM. *, $P < 0.05$; **, $P < 0.01$; n.s., not significant.

K). Thus, establishment of repression at an endogenous DSB site is not dependent on preexisting transcriptional activity. Importantly, our data also demonstrate that DSBs in G_1 phase cells both repress ongoing transcription and block induced expression of a neighboring gene, even in the presence of a potent activating signal.

One recent study implicated the c-Abl kinase in facilitating transcription at DSB sites (35). To ensure that c-Abl inhibition by imatinib is not the sole underlying mechanism

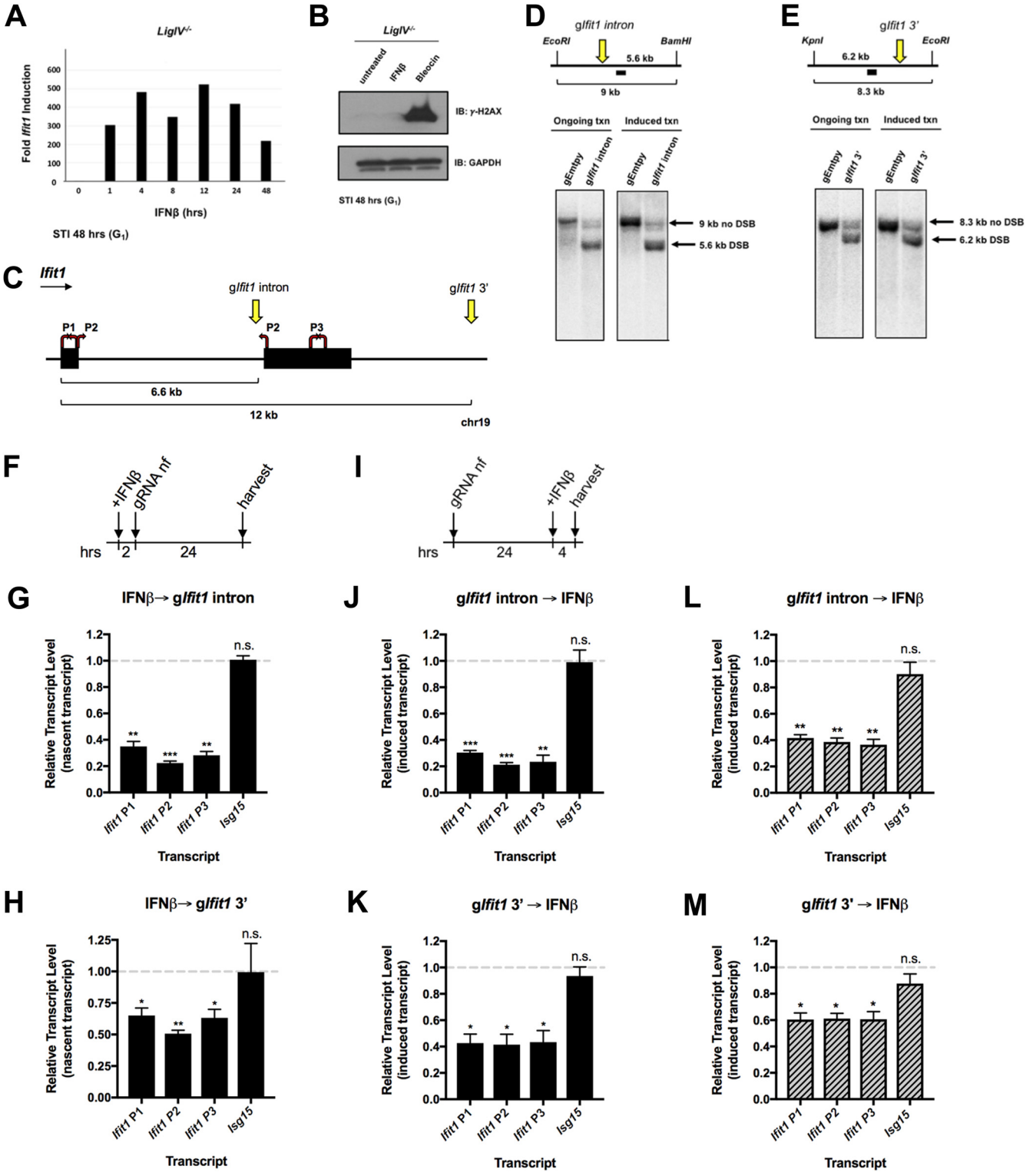

FIG 3 Persistent DSBs impede ongoing and induced transcription of an endogenous gene. (A) RT-qPCR analysis of total transcript levels of *Ifit1* (primer pair P2) in G_1-arrested *LigIV*$^{-/-}$ cells at the indicated time points after treatment with 100 U/ml IFN-β. The transcript levels relative to the levels in untreated cells (0-h time point) are shown. (B) Immunoblot (IB) analysis of γ-H2AX levels in G_1-arrested *LigIV*$^{-/-}$ cells that were untreated or treated with 100 U/ml IFN-β or 5 μg/ml of the DNA-damaging agent bleomycin (Bleocin) for 24 h. GAPDH expression is shown as a protein loading control. (C) Schematic of the *Ifit1* locus. gRNA target sites are denoted by yellow arrows, and the qPCR primers used to detect *Ifit1* transcripts are shown as red arrows. The distances between gRNA target sites and the *Ifit1* promoter are indicated. (D) Schematic of the Southern blotting strategy for detecting cleaved alleles at the *Ifit1* intronic gRNA target site (g*Ifit1* intron) (top) and Southern blots showing intact and cut *Ifit1* alleles at 24 h (left) or 28 h (right) after nucleofection of G_1-arrested, *LigIV*$^{-/-}$*:iCas9* cells with an empty gRNA vector (gEmpty) or the g*Ifit1* intron (bottom). Cells were treated with 100 U/ml IFN-β, as described in the work flow presented in panel F (left) or as described in the work flow presented in panel I (right). (E) Schematic of the Southern blotting strategy for detecting cleaved alleles at the *Ifit1 3'*

(Continued on next page)

for transcriptional repression in response to DSBs at an adjacent gene, we arrested *LigIV*$^{-/-}$*:iCas9* cells in G_1 using the CDK4/6 inhibitor palbociclib, which spares c-Abl activity (59). Both gene body and downstream breaks blocked *Ifit1* induction in palbociclib-treated cells, indicating that DSB-dependent repression of local gene transcription is independent of Abl kinase inhibition via imatinib (Fig. 3L and M).

Chromatin accessibility near persistent DSBs. A potential mechanism by which DSBs mediate transcriptional repression could be a break-induced loss of chromatin accessibility at nearby regulatory elements. In this regard, prior studies generally have concluded that DSBs enhance accessibility at DNA ends but lead to compaction of flanking chromatin (18, 36–38). However, the impact of a single DSB on chromatin accessibility at proximal regulatory elements remains unknown. The well-defined regulatory architecture of *Ifit1* afforded an ideal opportunity to test DSB-accessibility relationships.

For this purpose, we examined chromatin accessibility following the introduction of targeted *Ifit1* DSBs via the assay for transposase-accessible chromatin using sequencing (ATAC-seq). Cells harboring the *Ifit1* intronic break and treated with IFN-β, as outlined in Fig. 3I, exhibited enhanced accessibility for ~500 bp on either side of the DSB site (Fig. 4A). Notably, the *Ifit1* promoter remained accessible, despite potent transcriptional repression (Fig. 4A). Statistical comparison of global ATAC-seq data for control cells versus those for cells harboring an *Ifit1* intronic DSB revealed no significant changes in chromatin accessibility genome-wide, with the exception of the break site itself (Fig. 4B). We conclude that global chromatin accessibility remains remarkably stable in the presence of a DSB and that the break-induced block in *Ifit1* transcription is not driven by occlusion of its promoter.

DSB-dependent transcriptional repression extends to distal genes within the γ-H2AX domain. Previous studies have suggested that DSB-dependent transcriptional repression is limited to genes that are either directly damaged by a break or situated within a few kilobases of the lesion (18, 20, 21, 39, 40). Since DDR-signaling platforms in chromatin extend hundreds of kilobases from a break site, we hypothesized that transcriptional silencing might spread further in G_1 cells, perhaps throughout the γ-H2AX domain. The efficiency of DSB formation in v-Abl-transformed cells, coupled with unique features of the *Ifit* locus, namely, the proximity of several interferon-inducible genes, permits us to test more rigorously whether repression spreads beyond a directly adjacent gene.

Initially, we measured IFN-β-induced transcription of neighboring genes *Ifit3b*, *Ifit3*, and *Ifit2* (Fig. 5A) in cells harboring an intragenic *Ifit1* break. DSB-mediated repression extended to all of the inducible *Ifit* genes in this region, albeit to a lesser extent than *Ifit1* itself (Fig. 5B). Similarly, a DSB introduced into a second *Ifit* gene, *Ifit2*, blocked activation of the other IFN-β-inducible genes in this cluster (Fig. 5C). We conclude that regional repression is independent of the precise DSB location.

We next sought to determine if repression extended to more distal genes within the γ-H2AX domain in response to a DSB. The intronic break in *Ifit1* produced a γ-H2AX

FIG 3 Legend (Continued)
gRNA target site (g*Ifit1 3′*) (top) and Southern blots showing intact and cut *Ifit1* alleles, as described in the legend to panel D (bottom). (F) Work flow for the ongoing transcription experiments whose results are shown in panels G and H. (G) RT-qPCR analysis of nascent transcript levels of *Ifit1* (primer pairs P1, P2, and P3) and a control interferon-stimulated gene on a separate chromosome, *Isg15*, at 24 h after nucleofection with a gRNA targeting the *Ifit1* intron (g*Ifit1* intron). Cells were treated with 100 U/ml IFN-β 2 h prior to nucleofection and pulsed with EU 1 h prior to harvesting for RNA isolation. Nascent transcripts were isolated with the Click-iT nascent RNA capture technology. Transcript levels are shown relative to the levels in cells nucleofected with an empty gRNA vector. (H) RT-qPCR analysis of nascent transcript levels of *Ifit1*, as described in the legend to panel G, after nucleofection with a gRNA targeting the region ~3 kb downstream of the *Ifit1* gene body (g*Ifit1* 3′). (I) Work flow for the induced transcription experiments whose results are shown in panels J to M. (J) RT-qPCR analysis of induced transcript levels of *Ifit1* (primer pairs P1, P2, and P3) and *Isg15* at 28 h after nucleofection with a gRNA targeting the *Ifit1* intron (g*Ifit1* intron). Cells were treated with 100 U/ml IFN-β for 4 h at 24 h after nucleofection. Transcript levels are shown relative to the levels in cells nucleofected with gEmpty. (K) RT-qPCR analysis of induced transcript levels of *Ifit1*, as described in the legend to panel J, after nucleofection with g*Ifit1* 3′. (L) RT-qPCR analysis of induced transcript levels of *Ifit1* and *Isg15* in cells arrested in G_1 with palbociclib, followed by nucleofection and treatment, as described in the legend to panel J. (M) RT-qPCR analysis of induced transcript levels of *Ifit1* and *Isg15* in cells arrested in G_1 with palbociclib, followed by nucleofection and treatment, as described in the legend to panel K. Data from panels G, H, and J to M represent those from 3 independent experiments ($n = 3$). Error bars show the SEM. *, $P < 0.05$; **, $P < 0.01$; ***, $P < 0.001$; n.s., not significant. txn, transcription.

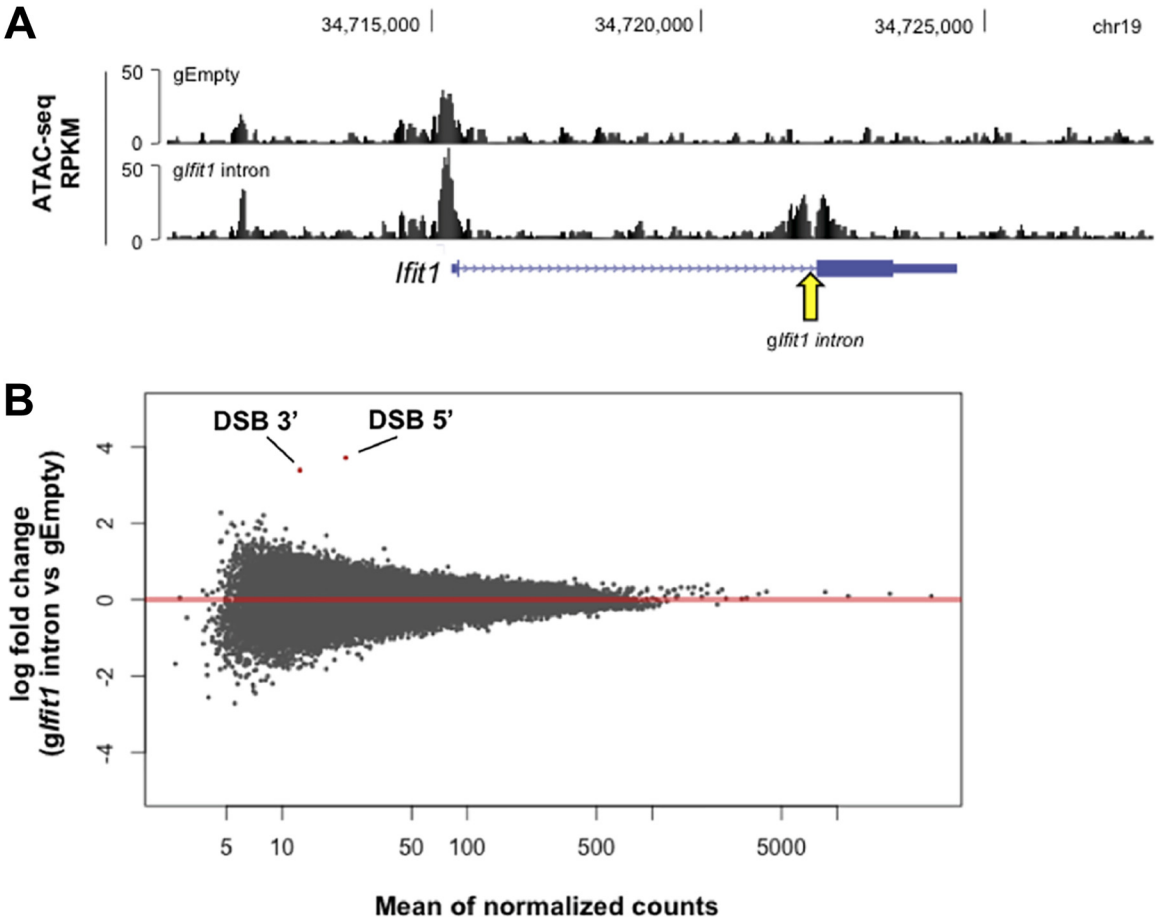

FIG 4 DSB-induced changes in chromatin accessibility are limited to the break site itself. (A) UCSC Genome Browser screenshot depicting the ATAC-seq signal at the *Ifit1* locus in G_1-arrested *LigIV*$^{-/-}$ v-Abl-transformed pre-B cells nucleofected with gEmpty (top track) and the g*Ifit1* intron (bottom track) and treated with IFN-β, as outlined in Fig. 3I. The arrow denotes the g*Ifit1* intron target site. (B) Plot depicting the $\log_2$ fold change of the read counts for each ATAC-seq peak and the mean of the normalized read counts for each peak between cells nucleofected with gEmpty and cells nucleofected with the g*Ifit1* intron and treated with IFN-β, as outlined in Fig. 3I (results are averages from three biological replicates [$n = 3$]). Each dot represents an individual ATAC-seq peak. Two peaks (indicated in red) are called significantly different by the DESeq2 program (Wald test, $P < 0.05$) and correspond to the peaks on either side of the *Ifit1* intronic DSB, as visualized in panel A.

domain that spread for several hundred kilobases on each side, as monitored by chromatin immunoprecipitation-DNA sequencing (ChIP-seq) (Fig. 5D). Two constitutively expressed genes, *Stambpl1* and *Kif20b*, are located near each end of the region decorated by γ-H2AX. Remarkably, we observed a significant reduction in the transcript levels of *Kif20b* (~40%), which is located ~275 kb away from the *Ifit1* DSB (Fig. 5E). The transcription of *Stambpl1*, whose promoter lies ~455 kb away from the *Ifit1* DSB, also was affected significantly, albeit to a lesser extent (~20%) (Fig. 5E). In contrast, the expression of two genes positioned on either side of the γ-H2AX domain, *Atad* and *Tnks2*, remained unchanged (Fig. 5F). Indeed, whole-transcriptome analysis of control versus *Ifit1* DSB samples revealed a significant DSB-dependent decrease in the expression of genes lying within the *Ifit1* γ-H2AX domain compared to all other genes (Fig. 5G). Furthermore, breaks at *Ifit2* elicited similar levels of *Stambpl1* and *Kif20b* repression (Fig. 5H). Thus, we conclude that DSB-induced transcriptional repression in an endogenous locus can spread for several hundred kilobases on either side of a break site throughout the γ-H2AX domain.

DSB-induced local gene silencing depends on the DNA damage response and reduced RNAPII activity. To determine whether the spread of gene repression from a DSB site requires DDR signaling, which generates γ-H2AX, we treated cells with

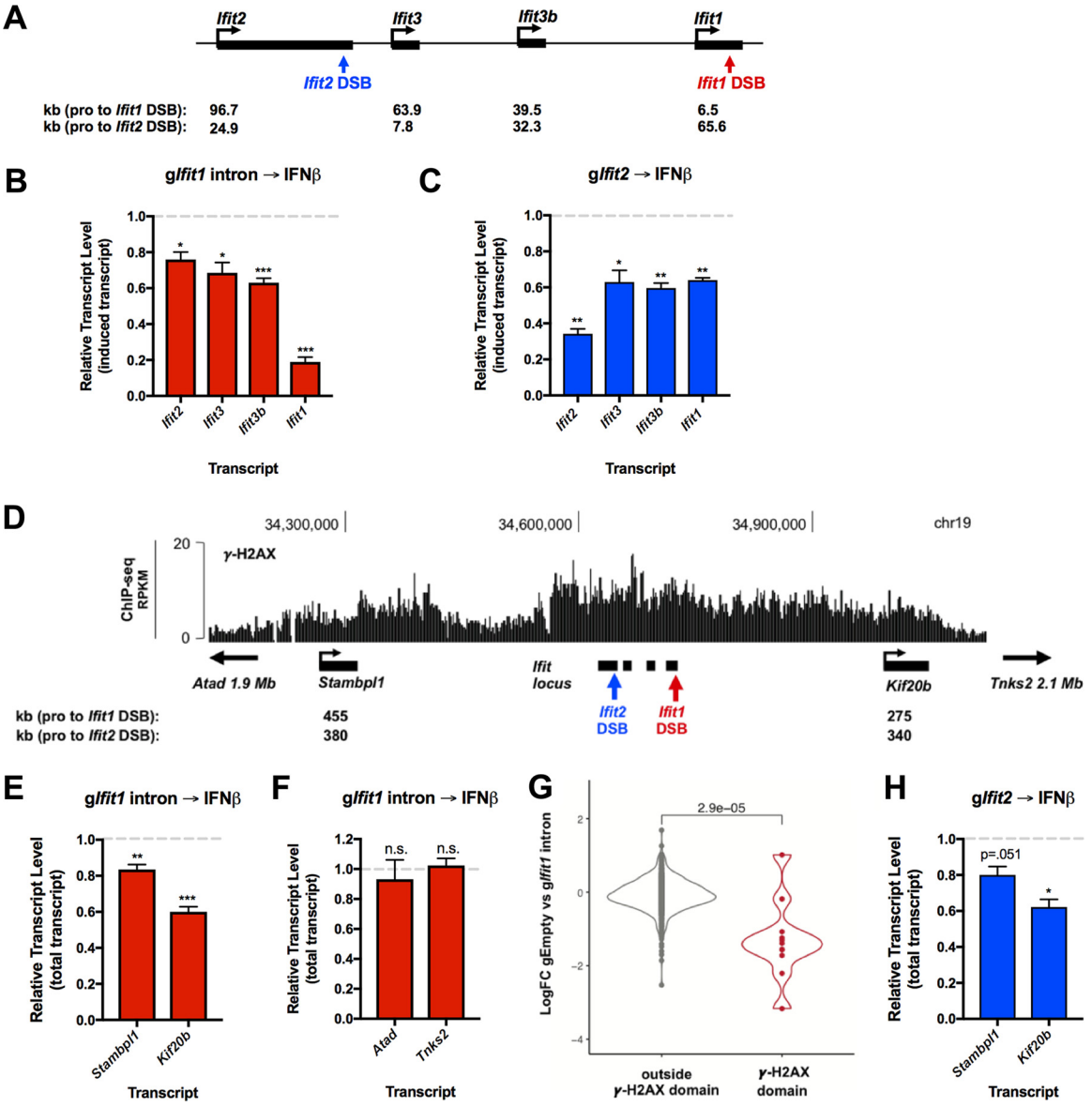

FIG 5 DSB-dependent transcriptional repression spreads to distal genes within the γ-H2AX domain. (A) Schematic of the *Ifit* locus. IFN-β-inducible genes (ISGs) are shown in black. The g*Ifit1* intron break site and the g*Ifit2* break site are denoted in red and blue, respectively. The distances from the promoters of each ISG and each DSB site are indicated below. (B) RT-qPCR analysis of induced transcript levels of *Ifit* locus ISGs in cells nucleofected with the g*Ifit1* intron. Transcript levels are shown relative to the levels in cells nucleofected with gEmpty and treated with IFN-β, as outlined in Fig. 3I. (C) RT-qPCR analysis of induced transcript levels of *Ifit* locus ISGs in cells nucleofected with gRNA targeting *Ifit2* exon 3 (g*Ifit2*). Transcript levels are shown relative to the levels in cells nucleofected with gEmpty and treated with IFN-β, as described in the legend to panel B. (D) UCSC Genome Browser screenshot depicting the γ-H2AX ChIP-seq signal at the *Ifit* locus in *LigIV*$^{-/-}$*:iCas9* cells at 24 h after nucleofection with the g*Ifit1* intron. Distal genes lying within the γ-H2AX domain are shown in black. The g*Ifit1* intron break site and the g*Ifit2* break site are denoted in red and blue, respectively. The distances from the promoters of each distal gene and each DSB site are indicated below. (E) RT-qPCR analysis of the total transcript levels of distal genes *Stambpl1* and *Kif20b* from the experiments whose results are presented in panel B. (F) RT-qPCR analysis of total transcript levels of *Atad* and *Tnks2* from the experiments whose results are presented in panel B. *Atad* and *Tnks2* are located upstream and downstream of the *Ifit1* DSB γ-H2AX domain, respectively. (G) Violin plot showing the mean $\log_2$ fold change of expression between cells nucleofected with gEmpty and cells nucleofected with the g*Ifit1* intron and treated with IFN-β, as outlined in Fig. 3I. Genes located within and outside the chromosome 19 *Ifit1* γ-H2AX peaks (D) are shown in red and gray, respectively. Each dot represents an individual gene. The Wilcoxon test was used to generate the *P* value. (H) RT-qPCR analysis of the total transcript levels of distal genes *Kif20b* and *Stambpl1* in cells nucleofected with gRNA targeting *Ifit2* exon 3 (g*Ifit2*) from the experiments whose results are presented in panel C. The data in panels B, E, and F represent those from 4 independent experiments ($n = 4$), the data in panels C and H represent those from 3 independent experiments ($n = 3$), and the data in panel G represent those from 1 biological replicate ($n = 1$). Error bars show the SEM. *, $P < 0.05$; **, $P < 0.01$; ***, $P < 0.001$; n.s., not significant.

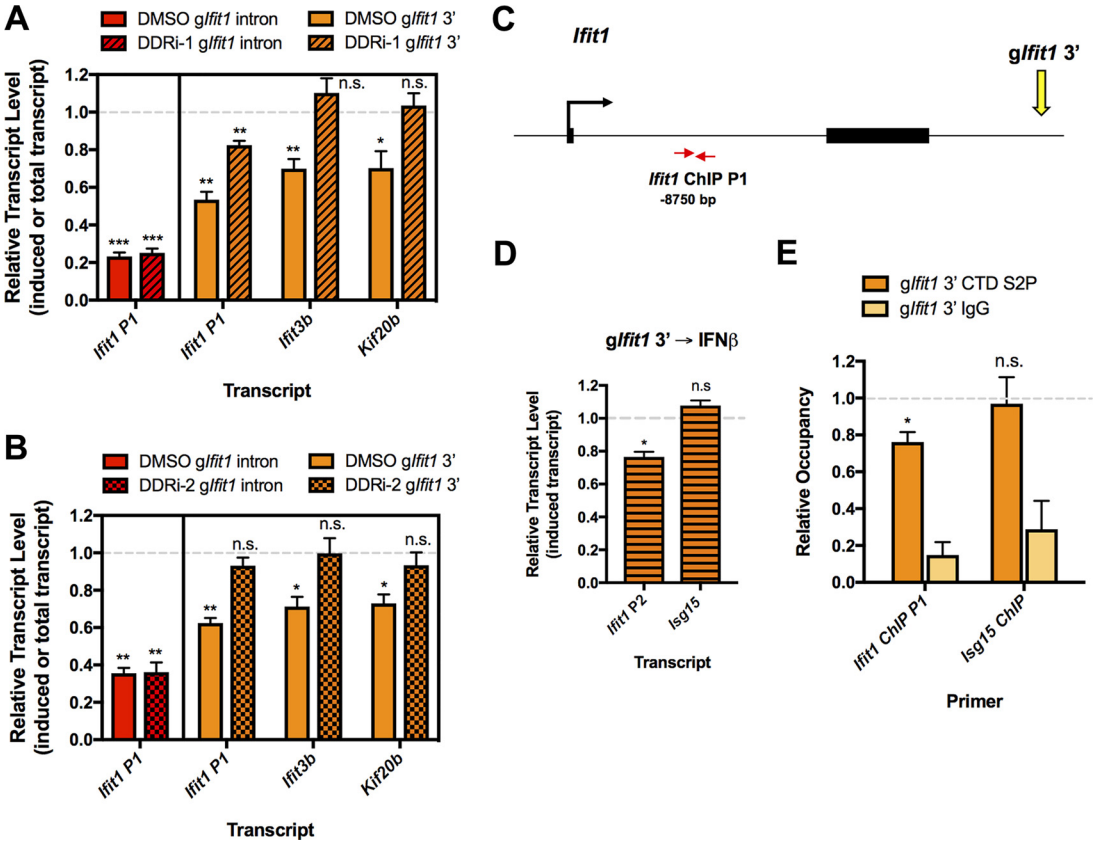

FIG 6 DSB-induced gene silencing depends on the DNA damage response and reduced RNAPII activity. (A) RT-qPCR analysis of the induced *Ifit1* transcript in cells nucleofected with the g*Ifit1* intron and of the induced *Ifit1* and *Ifit3b* transcript and the total *Kif20b* transcript in cells nucleofected with g*Ifit1* 3′. Cells were nucleofected and then transferred to medium containing DMSO or an ATM inhibitor (KU55933) and DNA-PKcs inhibitor (NU7026) (the DDRi-1 treatment) and treated with IFN-β, as outlined in Fig. 3I. Transcript levels in samples treated with DMSO or the DDRi are shown relative to the levels in cells nucleofected with gEmpty and treated with DMSO or DDRi, respectively. (B) RT-qPCR analysis, as described in the legend to panel A, for cells treated with DMSO or an ATM inhibitor (KU60019) and DNA-PKcs inhibitor (NU7441) (the DDRi-2 treatment). (C) Schematic depicting the *Ifit1* locus, g*Ifit1* 3′ target site, and *Ifit1* qPCR primer locations used for the ChIP analysis whose results are presented in panel E. The distance from the primers to the *Ifit1* 3′ gRNA target site is indicated. (D) RT-qPCR analysis of induced transcript levels of *Ifit1* (primer pair *Ifit1* P2) and *Isg15* at 26 h after nucleofection with g*Ifit1* 3′. Cells were treated with 100 U/ml IFN-β for 2 h at 24 h after nucleofection. Transcript levels are shown relative to the levels in cells nucleofected with gEmpty and treated with IFN-β. (E) ChIP analysis of RNAPII CTD S2P occupancy in the *Ifit1* gene from the experiments whose results are presented in panel D. RNAPII levels are presented relative to the levels in cells nucleofected with the empty gRNA vector (no DSBs). The relative RNAPII CTD S2P occupancy at the undamaged *Isg15* locus is shown as a control. The data in panel A represent those from 4 independent experiments ($n = 4$), the data in panel B represent those from three independent experiments ($n = 3$), and the data in panels D and E represent those from 3 independent experiments ($n = 3$). Error bars show the SEM. *, $P < 0.05$; **, $P < 0.01$; ***, $P < 0.001$; n.s., not significant.

combined ATM (KU55933) and DNA-PKcs (NU7026) inhibitors (DDR inhibitor 1 [DDRi-1] treatment) or the dimethyl sulfoxide (DMSO) vehicle immediately after gRNA nucleofection. The DDRi-1 treatment did not restore induced *Ifit1* mRNA levels in cells with *Ifit1* intronic DSBs, possibly because intragenic breaks lead to transcript instability (Fig. 6A). Consistent with this possibility, when a DSB was targeted outside of the *Ifit1* gene body (*Ifit1* 3′ DSB), The DDRi-1 treatment partially rescued its transcriptional activation (Fig. 6A). Notably, silencing of the IFN-β-inducible gene *Ifit3b* and of the constitutive gene *Kif20b* also was reversed by DDR inhibition (Fig. 6A). To further confirm that silencing is dependent on DDR signaling, we employed a second set of ATM (KU60019) and DNA-PKcs (NU7441) inhibitors (the DDRi-2 treatment), which led to a similar rescue of transcription at neighboring genes (Fig. 6B). Thus, DDR-dependent repression can spread for a significant distance from a DSB to suppress not only ongoing but also induced gene transcription in the resultant γ-H2AX domain.

Prior studies indicated that the levels of elongating or total RNA polymerase II (RNAPII) are reduced at genes adjacent to DSBs (18, 20, 21). However, it remains unclear

how RNAPII activity is affected at loci near persistent DSBs in G_1 phase cells. We thus measured the levels of elongating, C-terminal domain Ser2-phosphorylated (CTD S2P) RNAPII via chromatin immunoprecipitation (ChIP) in response to *Ifit1* downstream DSBs, as outlined in Fig. 3I. We chose to focus on DSBs outside the gene body, as they do not present a physical barrier to RNAPII progression. Because previous reports indicated that RNAPII levels at *Ifit1* were maximal at 2 h subsequent to interferon treatment, we assessed RNAPII CTD S2P occupancy at that time point (41). Indeed, we observed an ~20% reduction in transcript levels and a corresponding decrease in elongating RNAPII levels over the *Ifit1* gene compared to the levels in undamaged cells (Fig. 6C to E). As expected, the levels were unchanged at the *Isg15* control locus (Fig. 6D and E). Thus, we conclude that transcriptional repression of DSB-adjacent endogenous genes in G_1 phase occurs through a loss of RNAPII activity, corroborating previous findings in cycling cells at transcriptional reporter loci (18).

DISCUSSION

A major hurdle for understanding the functional consequences of DDR signaling in noncycling cells has been a lack of approaches to target DSBs at predetermined sites in native chromatin. Recently developed cellular systems have used endonucleases that cleave at a specific recognition sequence. However, the DSBs are limited to a small collection of naturally occurring sites that may not be ideal for studying certain aspects of the damage response. For example, AsiSI and I-PpoI cleave predominantly in promoter regions or ribosomal DNA repeats, respectively (20, 21, 39, 40). We established an experimental system that leverages the flexibility of the CRISPR/Cas9 technology to generate DSBs in NHEJ-deficient cells arrested in G_1 phase. Our approach was used to create site-specific DSBs with a high efficiency (50 to 90% broken alleles) at multiple, predetermined genomic sites, enabling us to interrogate transcriptional responses to persistent DSBs. By targeting breaks to multiple sites in the *Ifit1* locus, where transcription is regulated solely by promoter elements, we provide definitive evidence that DSBs can repress endogenous gene transcription in G_1 phase cells independently of damage to the gene body itself or its key regulatory elements.

These advances build on prior investigations of DSB-induced silencing, many of which employed systems that simultaneously generate multiple DSBs within gene bodies or near genes with ongoing transcriptional activity. Thus, although DSB-mediated repression of a proximal gene was observed in most cases, it remained unclear whether preexisting transcriptional activity at or near a break site was required for this functional outcome. Indeed, the RNA polymerase II-associated factors ENL and NELF-E have been implicated in DSB-induced repression in cycling cells; however, their recruitment to DSBs was dependent on active transcription near the break site (22, 42). Leveraging the inducible nature of *Ifit* genes, we show that DSBs not only repress ongoing gene expression but also block induced transcription, even when the lesion resides outside the transcriptional unit. This reduction of the induced *Ifit1* transcript in response to adjacent DSBs corresponds with the decreased levels of active RNAPII at *Ifit1*. Although the precise mechanisms of DSB-mediated gene repression remain an important unresolved question, they likely are independent of changes in chromatin accessibility at key regulatory elements, as revealed by our comparisons of ATAC-seq data for cells harboring intact or broken *Ifit* alleles.

An important finding to emerge from our approach is that DSB-mediated repression is not limited to a neighboring gene. Prior studies had suggested that transcriptional silencing is restricted to DSB-harboring or -proximal genes, without having a significant impact on other genes within a γ-H2AX domain (20, 21, 39, 40). In addition, the architectural complex cohesin was implicated in the protection of more distal γ-H2AX domain genes from DSB-mediated repression (43). We found that although transcriptional silencing required DDR signaling, repression could extend to significant distances from a DSB, even past CTCF-cohesin binding sites, ultimately attenuating expression of both inducible and constitutive genes throughout the resultant γ-H2AX domain. Although we cannot rule out the possibility that repression of the *Ifit* genes results from disruption

TABLE 1 gRNA sequences and oligonucleotides for cloning

gRNA name	gRNA sequence (5′–3′)	Oligonucleotide sequence for pKLV-BbsI cloning (5′–3′)[a]		Mouse chromosome
		Forward	Reverse	
g*Eb*	GAAAGCCAGCCAATGAATGC	CACCGAAAGCCAGCCAATGAATGCGT	TAAAACGCATTCATTGGCTGGCTTTC	6
g*Irf4* intron	GGCCAACCCTACACCCTAAA	CACCGGCCAACCCTACACCCTAAAGT	TAAAACTTTAGGGTGTAGGGTTGGCC	13
g*Irf4* 5′	AGGCTAGGTTACGACTAGAA	CACCGGGCTAGGTTACGACTAGAAGT	TAAAACTTCTAGTCGTAACCTAGCCC	13
g*Ifit1* intron	ATGGCCAGAAATGGACACCG	CACCGTGGCCAGAAATGGACACCGGT	TAAAACCGGTGTCCATTTCTGGCCAC	19
g*Ifit1* 3′	CTGTTCTGCTACCTGCCGAG	CACCGTGTTCTGCTACCTGCCGAGGT	TAAAACCTCGGCAGGTAGCAGAACAC	19
g*Ifit2*	CAGACTTCCAGGAGTCGCAT	CACCGAGACTTCCAGGAGTCGCATGT	TAAAACATGCGACTCCTGGAAGTCTC	19

[a]Underlined text denotes sequences appended for cloning into the pKLV-U6gRNA(BbsI)-UbcThy1.1 (pKLV-BbsI) gRNA expression vector.

of a transcriptional coregulatory mechanism within this locus and not the DSB *per se*, the observed repression of the distal genes *Kif20b* and *Stambpl1* suggests bona fide DSB-dependent long-range gene silencing. Curiously, topoisomerase II (TOP2) localizes to chromatin loop anchors, where it relieves torsional strain through the formation of transient, TOP2-linked DNA breaks (44, 45). DSB intermediates in TOP2 cleavage complexes (TOP2ccs) are thought to be shielded from the DNA surveillance machinery and do not elicit a DDR (2). Perhaps this cloaking mechanism prevents the regional transcriptional repression that may be necessary for the efficient and accurate repair of genotoxic DSBs but not these transient, TOP2-associated breaks.

While it is unclear if γ-H2AX itself is essential for this mode of transcriptional repression, the histone modification serves as a proxy that highlights the reaches of DDR signaling. Intriguingly, ATM recruitment may be restricted to only a short stretch of chromatin near endogenous DSB sites, suggesting that DDR signaling spreads through megabase-size domains via contacts between the break and more distal sites, rather than through direct linear propagation (46). Moreover, DSBs appear to boost *cis* interactions within γ-H2AX domains, as revealed using a chromosome conformation capture-based technique (capture-HiC) (47). In agreement with the results of these studies, we observed a nonuniform distribution of γ-H2AX from our *Ifit1* DSB. This finding, together with our transcriptional data, raises the compelling possibility that DSBs enhance the contacts of surrounding chromatin with ATM loaded near the damaged site to spread DDR signaling and impose transcriptional silencing at more distal genes. As transcriptionally active regions are prone to DSBs, it is conceivable that active repression of genes is important for minimizing the appearance of additional DSBs within a confined region, thus limiting the risk of genomic rearrangements. Our approach, which generates targeted endogenous DSBs and a sustained DDR signaling response, should provide a means to rigorously test such hypotheses in the future. Indeed, the inherent flexibility of this system should lead to a deeper understanding of factors that facilitate the spread of DDR signaling to distal sites, as well as its full impact on regional transcription, chromatin landscapes, and repair.

MATERIALS AND METHODS

Cell culture. *LigIV*$^{-/-}$ v-Abl-transformed pre-B cells were described previously (31, 32). pCW-Cas9 (catalog number 50661; Addgene) was used to generate *LigIV*$^{-/-}$ v-Abl-transformed pre-B cell lines with a stably integrated, doxycycline-inducible Cas9 (*LigIV*$^{-/-}$*:iCas9* cells). For Cas9 induction, *LigIV*$^{-/-}$*:iCas9* cells were treated with 6 μg/ml doxycycline (Sigma) for 12 h prior to G_1 arrest using imatinib (3 μM, 10^6 cells/ml) or palbociclib (5 μM, 10^6 cells/ml). Murine IFN-β (100 U/ml; PBL Assay Science) was used to upregulate IFN-β-inducible gene (ISG) expression. For DDR inhibitor experiments, cells were treated with 30 μM ATM kinase inhibitor KU55933 (Tocris) and 20 μM DNA-PKcs inhibitor NU7026 (Selleck) (the DDRi-1 treatment) or with 2 μM ATM kinase inhibitor KU60019 (Selleck) and 4 μM DNA-PKcs inhibitor NU7441 (Selleck) (the DDRi-2 treatment) directly after nucleofection. The duration of the treatments for each experiment is indicated in the text and figures.

Plasmids. To generate the pKLV-U6gRNA(BbsI)-UbcThy1.1 gRNA expression vector, pKLV-U6gRNA(BbsI)-PGKpuro2ABFP (catalog number 50946; Addgene) was digested with BamHI and NotI to remove the PGKpuro2ABFP cassette and replace it with a Ubc-Thy1.1 cassette. The BbsI site in the Ubc promoter sequence was destroyed via site-directed mutagenesis. gRNA sequences were cloned into the BbsI gRNA cloning site as previously described (48).

gRNA design. All gRNA sequences were designed using the MIT CRISPR design tool, with the exception of g*Eb*, which was previously published (49, 50). The gRNA sequences and oligonucleotide sequences used for cloning into pKLV-U6gRNA(BbsI)-UbcThy1.1 vector are listed in Table 1.

TABLE 2 Southern blot restriction digests and probe sequences

gRNA target site	Restriction digestion enzyme(s)	Oligonucleotide sequence (5′–3′)	
		Forward probe	Reverse probe
Eb	HindIII	CTAGTCCCATCACCTAAGTCCCAG	GTCAGCAAATGTTCATAGAGC
Irf4 intron	KpnI	GGCCTCAGTCTGTGTGGGG	GAGAGCCCAGCTAGCATGGG
Irf4 5′	BamHI	GCATTGTCCTACCTCCAAAGAC	CTAGGTTCCTTATGACCATGG
Ifit1 intron	EcoRI/BamHI	GCCATTCATGAATTTCAAGAGAC	GAGCCTCAGTGCCTTCTCATAG
Ifit1 3′	KpnI/EcoRI	GCCATTCATGAATTTCAAGAGAC	GAGCCTCAGTGCCTTCTCATAG

Nucleofection. *LigIV*$^{-/-}$*:iCas9* cells were treated with doxycycline for 36 h and imatinib for 24 h prior to nucleofection. For each nucleofection, 20×10^6 cells were spun down and resuspended in 100 μl Nucleofector solution for human B cells (Lonza) or Chica buffer 1SM (51). Nucleofections were performed using an Amaxa Nucleofector II device (Lonza), program X-001, according to the manufacturer's instructions. Nucleofected cells were transferred directly to preequilibrated recovery medium containing doxycycline and imatinib at 10×10^6 cells/ml and incubated for 24 h prior to harvesting for RNA and genomic DNA. For induced *Ifit* expression experiments, cells were treated with IFN-β for 4 h prior to harvest. IFN-β was added to the cell cultures at 2 h before nucleofection and to the recovery medium for ongoing transcription experiments with DSBs at the *Ifit1* locus. For DDR inhibitor experiments, cells were transferred directly to recovery medium containing ATM and DNA-PKcs inhibitors or DMSO.

Southern blotting. Southern blotting of Cas9 DSBs was performed as previously described (50). Briefly, genomic DNA was isolated from 5×10^6 cells at the time points indicated above and in the figures, and 10 μg of gDNA was used for digestion with the restriction enzyme. The restriction digestion enzymes and oligonucleotides used for amplification of the probes from genomic DNA for each Southern blotting/DSB site are listed in Table 2.

Intracellular staining. Intracellular staining was performed using a BD Cytofix/Cytoperm fixation/permeabilization solution kit (Thermo Fisher) according to the manufacturer's instructions. The primary antibody used was anti-FLAG M2 (catalog number F1804; Sigma).

Flow cytometric analysis. Flow cytometric analyses were performed using a BD FACSCalibur flow cytometer (BD Biosciences), and the data were analyzed using FlowJo software (FlowJo, LLC). The antibodies used were phycoerythrin-conjugated anti-rat CD90/mouse CD90.1 (catalog number 205903; BioLegend) and Alexa Fluor 647-conjugated goat anti-mouse IgG (catalog number A-21235; Invitrogen).

Immunoblot analysis. Whole-cell lysates were prepared using LDS sample buffer (Invitrogen). Standard immunoblotting techniques were used, as previously described (32). The primary antibodies used were anti-γ-H2AX (catalog number 05-636; Millipore) and anti-GAPDH (anti-glyceraldehyde-3-phosphate dehydrogenase; catalog number sc-365062; Santa Cruz).

Total RNA isolation, cDNA synthesis, and RT-qPCR analysis. Total RNA was isolated from 5×10^6 to 10×10^6 cells with the TRIzol reagent and DNase treated in solution for 10 min (Qiagen RNase-free DNase set) to remove any remaining genomic DNA. DNase-treated RNA was then purified using Qiagen RNeasy columns. Purified RNA was quantified using a NanoDrop 2000 spectrophotometer, and cDNA was synthesized from 1 μg of RNA with random hexamers using SuperScript III reverse transcriptase (Thermo Fisher). Gene expression was assessed by qPCR using the Sybr green reagent (Sigma) and a Bio-Rad CFX Connect real-time PCR detection system. A β-2-microglobulin transcript was used as a normalization control for gene expression. The primers used for RT-qPCR analyses are listed in Table 3.

TABLE 3 RT-qPCR and ChIP-qPCR primer sequences

Primer name	Oligonucleotide sequence (5′–3′)	
	Forward	Reverse
β-2-Microglobulin	GGTCTTTCTGGTGCTTGTCTCA	GTTCGGCTTCCCATTCTCC
Irf4 P1	AAGCAGGACTACAATCGTGAG	TCGGAACTTGCCTTTAAACAATG
Irf4 P2	CAGAGACAGAGGAAGCTCATC	GTGTTCAGGTAACTCGTAGCC
Ifit1 P1	CAAGAGAGCAGAGAGTCAAGG	GTGGTAGCTGTTCTCTGGG
Ifit1 P2	AGAGTCAAGGCAGGTTTCTG	TGTGAAGTGACATCTCAGCTG
Ifit1 P3	TCTAGCAGGCAATTCCATCC	TCCAAAGGCACAGACATAAGG
Ifit3	CCTCTGCTCATCCTAGCCATACA	GTGCTCTGTCTGCTTTAAGCTC
Ifit3b	GAGGTTAAACAGCAAACATAGG	CCCTAACCCATTCAGCCACTC
Ifit2	CATTAGAAGGCAGAGGAAGAGG	GGCATTTTAGCTGTCGCAG
Kif20b	AGGAAGTGGAATTCTGCAGG	AAAACGTAAGACGGTCTAGGC
Stambpl1	CCGAGATGAAGTGACTGAGAAG	CTGTATGGTCAGGCATAGCAG
Atad	GACCACGAAGCTACAGCGAT	CTTGAGGGCGATTGGTAG
Tnks2	ACCCAAATGCTCGGGATAAT	GGCTCAGCTCCATGCTGTAA
Isg15	GCAGACTCCTTAATTCCAGGG	TTCAGTTCTGACACCGTCATG
Ifit1 ChIP P1	GGCATCTTCCTTCCATTACTTG	GACCACAGAAAGAGCATCAGTG
Isg15 ChIP	CCACAGCAACATCTATGAGGTC	ACTGGTCTTCGTGGACTTGTTC

Nascent RNA isolation. Nascent RNA was isolated using a Click-iT nascent RNA capture kit (Thermo Fisher) following the manufacturer's instructions. Briefly, cells were pulsed with 0.5 mM 5-ethynyl uridine (EU) for 1 h, and total RNA was harvested using the TRIzol reagent. One microgram of total RNA was used for the biotinylation reaction, and 300 ng of biotinylated RNA was captured on streptavidin-coated magnetic beads. cDNA was synthesized using captured, bead-bound RNA as a template with a SuperScript VILO cDNA synthesis kit (Thermo Fisher). qPCR analysis of cDNA from nascent transcripts was carried out as described above for total RNA.

Statistical analyses. Graphs for RT-qPCR and ChIP-qPCR data were generated and statistical analyses were performed using Prism (version 7) software (GraphPad). The transcript levels for samples nucleofected with a targeting gRNA vector were normalized to the transcript levels for the corresponding samples nucleofected with an empty gRNA control vector (gEmpty), and a one-sample *t* test was performed with a hypothetical mean set to 1. For each ChIP sample, the percentage of the input signal obtained using qPCR was determined. Data are expressed as relative occupancy (percent input relative to that for the gEmpty [no DSB] RNAPII CTD S2P ChIP sample), and a one-sample *t* test was performed with a hypothetical mean set to 1. *P* values below 0.05 were considered statistically significant.

ChIP-qPCR. ChIP assays were done as described previously, with the following modifications (52). Briefly, 30 μl protein A Dynabeads (Thermo Fisher) per immunoprecipitation (IP) was preincubated with 3 μg RNA polymerase II CTD repeat (phospho-S2) antibody (catalog number ab5095; Abcam) or 3 μg normal rabbit IgG antibody (catalog number 12-370; Millipore) overnight at 4°C. A total of 10×10^6 cells per IP were fixed using 1% formaldehyde at room temperature for 10 min, and then the reaction was quenched with 0.125 M glycine. Isolated nuclei were lysed and sonicated to a 200- to 500-bp average DNA fragment size using a Covaris M220 focused ultrasonicator (duration, 30 min; peak incident power [PIP], 75 W; duty factor, 10%; cycles per burst, 200 cycles; temperature, 6°C). Cleared lysates were incubated with antibody-Dynabeads overnight and then washed and eluted as previously described (52). Eluted DNA was analyzed by qPCR using the Sybr green reagent (Sigma) and a Bio-Rad CFX Connect real-time PCR detection system. The primers used for ChIP-qPCR analyses are listed in Table 3. Data represent the averages from three biological replicates.

ChIP-seq. ChIP assays were done as described previously (52). Briefly, 50 μl protein G Dynabeads (Thermo Fisher) per IP was preincubated with 2 μg γ-H2AX antibody (catalog number 05-636; Millipore) overnight at 4°C. A total of 3×10^6 cells per IP were fixed using 1% formaldehyde at room temperature for 10 min, and then the reaction was quenched with 0.125 M glycine. Isolated nuclei were lysed and sonicated to a 200- to 500-bp average DNA fragment size using a Diagenode Bioruptor Pico sonication device (60 cycles; 30 s on and 30 s off). Cleared lysates were incubated with antibody-Dynabeads overnight and then washed and eluted as previously described (52).

ATAC-seq. Fifty thousand cells per sample were counted, collected, and then washed once in cold phosphate-buffered saline. The cells were then spun down and resuspended in ATAC lysis buffer (10 mM Tris-HCl [pH 7.4], 10 mM NaCl, 3 mM $MgCl_2$, 0.1% IGEPAL CA-630) to isolate the nuclei. Samples prepared as described above were purified using MinElute spin columns (Qiagen). Nextera index adapters (i7 and i5) were used to amplify transposed DNA fragments per the manufacturer's protocol (Illumina).

RNA-seq. Total RNA was isolated from *LigIV*$^{-/-}$*:iCas9* cells nucleofected with the g*Ifit1* intron or gEmpty and treated with IFN-β as outlined in Fig. 3I and as described above. rRNA was depleted using a Ribo-Zero rRNA removal kit (Illumina). Transcriptome sequencing (RNA-seq) libraries were prepared as previously described and sequenced using an Illumina HiSeq 2500 1×50 system (53).

Data processing. ChIP-seq, ATAC-seq, and RNA-seq libraries were prepared as previously described and sequenced using an Illumina HiSeq 2500 1×50 system (ChIP) or a HiSeq 3000 2×150 system (ATAC) (53). The demultiplexed libraries were aligned using the NovaAlign tool, processed for normalization of the number of reads per kilobase per million (RPKM) using DeepTool's BamCoverage tool, and visualized on the UCSC Genome Browser (54, 55). Peaks were called using the Bowtie2 program (56). For ATAC analysis, the peaks were concatenated and merged using the BEDtools program, and then the reads were counted using DeepTool's multiBamSummary tool (57). Statistically significant ATAC regions were determined using the DEseq2 program (58). For RNA-seq analysis, genes overlapping γ-H2AX peaks were determined using BEDtools. DeepTool's BamCoverage tool was used to determined RPKM-normalized expression within or outside γ-H2AX peaks. The R package gpubR was used to statistically analyze and visualize the relative fold changes between sample groups.

ACKNOWLEDGMENTS

This work was supported by NIH grants R01 AI118852, R01 AI130231, and R01 AI134035 (to E.M.O.), R01 AI074953 (to B.P.S.), and T32 CA113275 and F31 CA203107 (to C.E.P.). The Genome Technology Access Center, Department of Genetics, WUSM, is partially supported by NCI Cancer Center support grant P30 CA91842 to the Siteman Cancer Center and by ICTS/CTSA grant UL1TR000448 from the National Center for Research Resources (NCRR).

We thank the Genome Technology Access Center, Department of Genetics, WUSM, for the genomic analyses.

REFERENCES

1. Ciccia A, Elledge SJ. 2010. The DNA damage response: making it safe to play with knives. Mol Cell 40:179–204. https://doi.org/10.1016/j.molcel.2010.09.019.
2. Tubbs A, Nussenzweig A. 2017. Endogenous DNA damage as a source of genomic instability in cancer. Cell 168:644–656. https://doi.org/10.1016/j.cell.2017.01.002.
3. Bassing CH, Alt FW. 2004. The cellular response to general and programmed DNA double strand breaks. DNA Repair (Amst) 3:781–796. https://doi.org/10.1016/j.dnarep.2004.06.001.
4. Kass EM, Jasin M. 2010. Collaboration and competition between DNA double-strand break repair pathways. FEBS Lett 584:3703–3708. https://doi.org/10.1016/j.febslet.2010.07.057.
5. Chapman JR, Taylor MRG, Boulton SJ. 2012. Playing the end game: DNA double-strand break repair pathway choice. Mol Cell 47:497–510. https://doi.org/10.1016/j.molcel.2012.07.029.
6. Bunting SF, Nussenzweig A. 2013. End-joining, translocations and cancer. Nat Rev Cancer 13:443–454. https://doi.org/10.1038/nrc3537.
7. Sallmyr A, Giovannangeli C, Ruis B, Renaud J-B, Renouf B, Oh S, Tomkinson AE, Ghezraoui H, Brunet E, Piganeau M, Jasin M, Hendrickson EA. 2014. Chromosomal translocations in human cells are generated by canonical nonhomologous end-joining. Mol Cell 55:829–842. https://doi.org/10.1016/j.molcel.2014.08.002.
8. Biehs R, Steinlage M, Barton O, Juhász S, Künzel J, Spies J, Shibata A, Jeggo PA, Löbrich M. 2017. DNA double-strand break resection occurs during non-homologous end joining in G1 but is distinct from resection during homologous recombination. Mol Cell 65:671–684.e5. https://doi.org/10.1016/j.molcel.2016.12.016.
9. Bredemeyer AL, Helmink BA, Innes CL, Calderon B, McGinnis LM, Mahowald GK, Gapud EJ, Walker LM, Collins JB, Weaver BK, Mandik-Nayak L, Schreiber RD, Allen PM, May MJ, Paules RS, Bassing CH, Sleckman BP. 2008. DNA double-strand breaks activate a multi-functional genetic program in developing lymphocytes. Nature 456:819–823. https://doi.org/10.1038/nature07392.
10. Zhou B-B, Elledge SJ. 2000. The DNA damage response: putting checkpoints in perspective. Nature 408:433–439. https://doi.org/10.1038/35044005.
11. Price BD, D'Andrea AD. 2013. Chromatin remodeling at DNA double-strand breaks. Cell 152:1344–1354. https://doi.org/10.1016/j.cell.2013.02.011.
12. Blackford AN, Jackson SP. 2017. ATM, ATR, and DNA-PK: the trinity at the heart of the DNA damage response. Mol Cell 66:801–817. https://doi.org/10.1016/j.molcel.2017.05.015.
13. Lee J-H, Paull TT. 2004. Direct activation of the ATM protein kinase by the Mre11/Rad50/Nbs1 complex. Science 304:93–96. https://doi.org/10.1126/science.1091496.
14. Goodarzi AA, Jeggo PA. 2013. The repair and signaling responses to DNA double-strand breaks. Adv Genet 82:1–45. https://doi.org/10.1016/B978-0-12-407676-1.00001-9.
15. Savic V, Yin B, Maas NL, Bredemeyer AL, Carpenter AC, Helmink BA, Yang-Iott KS, Sleckman BP, Bassing CH. 2009. Formation of dynamic gamma-H2AX domains along broken DNA strands is distinctly regulated by ATM and MDC1 and dependent upon H2AX densities in chromatin. Mol Cell 34:298–310. https://doi.org/10.1016/j.molcel.2009.04.012.
16. Kinner A, Wu W, Staudt C, Iliakis G. 2008. H2AX in recognition and signaling of DNA double-strand breaks in the context of chromatin. Nucleic Acids Res 36:5678–5694. https://doi.org/10.1093/nar/gkn550.
17. van Attikum H, Gasser SM. 2009. Crosstalk between histone modifications during the DNA damage response. Trends Cell Biol 19:207–217. https://doi.org/10.1016/j.tcb.2009.03.001.
18. Shanbhag NM, Rafalska-Metcalf IU, Balane-Bolivar C, Janicki SM, Greenberg RA. 2010. ATM-dependent chromatin changes silence transcription in cis to DNA double-strand breaks. Cell 141:970–981. https://doi.org/10.1016/j.cell.2010.04.038.
19. Kakarougkas A, Ismail A, Chambers AL, Riballo E, Herbert AD, Künzel J, Löbrich M, Jeggo PA, Downs JA. 2014. Requirement for PBAF in transcriptional repression and repair at DNA breaks in actively transcribed regions of chromatin. Mol Cell 55:723–732. https://doi.org/10.1016/j.molcel.2014.06.028.
20. Iannelli F, Galbiati A, Capozzo I, Nguyen Q, Magnuson B, Michelini F, D'Alessandro G, Cabrini M, Roncador M, Francia S, Crosetto N, Ljungman M, Carninci P, d'Adda di Fagagna F. 2017. A damaged genome's transcriptional landscape through multilayered expression profiling around in situ-mapped DNA double-strand breaks. Nat Commun 8:15656–15657. https://doi.org/10.1038/ncomms15656.
21. Pankotai T, Bonhomme C, Chen D, Soutoglou E. 2012. DNAPKcs-dependent arrest of RNA polymerase II transcription in the presence of DNA breaks. Nat Struct Mol Biol 19:276–282. https://doi.org/10.1038/nsmb.2224.
22. Ui A, Nagaura Y, Yasui A. 2015. Transcriptional elongation factor ENL phosphorylated by ATM recruits polycomb and switches off transcription for DSB repair. Mol Cell 58:468–482. https://doi.org/10.1016/j.molcel.2015.03.023.
23. Hustedt N, Durocher D. 2016. The control of DNA repair by the cell cycle. Nat Cell Biol 19:1–9. https://doi.org/10.1038/ncb3452.
24. Shaltiel IA, Krenning L, Bruinsma W, Medema RH. 2015. The same, only different—DNA damage checkpoints and their reversal throughout the cell cycle. J Cell Sci 128:607–620. https://doi.org/10.1242/jcs.163766.
25. Chakraborty A, Tapryal N, Venkova T, Horikoshi N, Pandita RK, Sarker AH, Sarkar PS, Pandita TK, Hazra TK. 2016. Classical non-homologous end-joining pathway utilizes nascent RNA for error-free double-strand break repair of transcribed genes. Nat Commun 7:13049. https://doi.org/10.1038/ncomms13049.
26. Lu W-T, Hawley BR, Skalka GL, Baldock RA, Smith EM, Bader AS, Malewicz M, Watts FZ, Wilczynska A, Bushell M. 2018. Drosha drives the formation of DNA:RNA hybrids around DNA break sites to facilitate DNA repair. Nat Commun 9:532. https://doi.org/10.1038/s41467-018-02893-x.
27. Cohen S, Puget N, Lin Y-L, Clouaire T, Aguirrebengoa M, Rocher V, Pasero P, Canitrot Y, Legube G. 2018. Senataxin resolves RNA:DNA hybrids forming at DNA double-strand breaks to prevent translocations. Nat Commun 9:533. https://doi.org/10.1038/s41467-018-02894-w.
28. Aguilera A, Gómez-González B. 2017. DNA-RNA hybrids: the risks of DNA breakage during transcription. Nat Struct Mol Biol 24:439–443. https://doi.org/10.1038/nsmb.3395.
29. Marnef A, Cohen S, Legube G. 2017. Transcription-coupled DNA double-strand break repair: active genes need special care. J Mol Biol 429:1277–1288. https://doi.org/10.1016/j.jmb.2017.03.024.
30. Meisenberg C, Pinder SI, Hopkins SR, Wooller SK, Benstead-Hume G, Pearl FMG, Jeggo PA, Downs JA. 2019. Repression of transcription at DNA breaks requires cohesin throughout interphase and prevents genome instability. Mol Cell 73:212–223.e7. https://doi.org/10.1016/j.molcel.2018.11.001.
31. Bredemeyer AL, Sharma GG, Huang C-Y, Helmink BA, Walker LM, Khor KC, Nuskey B, Sullivan KE, Pandita TK, Bassing CH, Sleckman BP. 2006. ATM stabilizes DNA double-strand-break complexes during V(D)J recombination. Nature 442:466–470. https://doi.org/10.1038/nature04866.
32. Helmink BA, Tubbs AT, Dorsett Y, Bednarski JJ, Walker LM, Feng Z, Sharma GG, McKinnon PJ, Zhang J, Bassing CH, Sleckman BP. 2011. H2AX prevents CtIP-mediated DNA end resection and aberrant repair in G1-phase lymphocytes. Nature 469:245–249. https://doi.org/10.1038/nature09585.
33. Fensterl V, Sen GC. 2011. The ISG56/IFIT1 gene family. J Interferon Cytokine Res 31:71–78. https://doi.org/10.1089/jir.2010.0101.
34. Flammer JR, Dobrovolna J, Kennedy MA, Chinenov Y, Glass CK, Ivashkiv LB, Rogatsky I. 2010. The type I interferon signaling pathway is a target for glucocorticoid inhibition. Mol Cell Biol 30:4564–4574. https://doi.org/10.1128/MCB.00146-10.
35. Burger K, Schlackow M, Gullerova M. 2019. Tyrosine kinase c-Abl couples RNA polymerase II transcription to DNA double-strand breaks. Nucleic Acids Res 47:3467–3484. https://doi.org/10.1093/nar/gkz024.
36. Marnef A, Legube G. 2017. Organizing DNA repair in the nucleus: DSBs hit the road. Curr Opin Cell Biol 46:1–8. https://doi.org/10.1016/j.ceb.2016.12.003.
37. Goldstein M, Derheimer FA, Tait-Mulder J, Kastan MB. 2013. Nucleolin mediates nucleosome disruption critical for DNA double-strand break repair. Proc Natl Acad Sci U S A 110:16874–16879. https://doi.org/10.1073/pnas.1306160110.
38. Li X, Tyler JK. 2016. Nucleosome disassembly during human non-homologous end joining followed by concerted HIRA- and CAF-1-dependent reassembly. Elife 5:e15129. https://doi.org/10.7554/eLife.15129.
39. Iacovoni JS, Caron P, Lassadi I, Nicolas E, Massip L, Trouche D, Legube G. 2010. High-resolution profiling of gammaH2AX around DNA double strand breaks in the mammalian genome. EMBO J 29:1446–1457. https://doi.org/10.1038/emboj.2010.38.
40. Kim J, Sturgill D, Tran AD, Sinclair DA, Oberdoerffer P. 2015. Controlled DNA double-strand break induction in mice reveals post-damage tran-

scriptome stability. Nucleic Acids Res 44:e64. https://doi.org/10.1093/nar/gkv1482.
41. Mostafavi S, Yoshida H, Moodley D, LeBoité H, Rothamel K, Raj T, Ye CJ, Chevrier N, Zhang S-Y, Feng T, Lee M, Casanova J-L, Clark JD, Hegen M, Telliez J-B, Hacohen N, De Jager PL, Regev A, Mathis D, Benoist C. 2016. Parsing the interferon transcriptional network and its disease associations. Cell 164:564–578. https://doi.org/10.1016/j.cell.2015.12.032.
42. Awwad SW, Abu-Zhayia ER, Guttmann-Raviv N, Ayoub N. 2017. NELF-E is recruited to DNA double-strand break sites to promote transcriptional repression and repair. EMBO Rep 18:745–764. https://doi.org/10.15252/embr.201643191.
43. Caron P, Aymard F, Iacovoni JS, Briois S, Canitrot Y, Bugler B, Massip L, Losada A, Legube G. 2012. Cohesin PROTECTS GENES against γH2AX induced by DNA double-strand breaks. PLoS Genet 8:e1002460. https://doi.org/10.1371/journal.pgen.1002460.
44. Canela A, Maman Y, Jung S, Wong N, Callen E, Day A, Kieffer-Kwon K-R, Pekowska A, Zhang H, Rao SSP, Huang S-C, Mckinnon PJ, Aplan PD, Pommier Y, Aiden EL, Casellas R, Nussenzweig A. 2017. Genome organization drives chromosome fragility. Cell 170:507–521.e18. https://doi.org/10.1016/j.cell.2017.06.034.
45. Fowler F, Tyler JK. 2017. Anchoring chromatin loops to cancer. Dev Cell 42:209–211. https://doi.org/10.1016/j.devcel.2017.07.013.
46. Caron P, Choudjaye J, Clouaire T, Bugler B, Daburon V, Aguirrebengoa M, Mangeat T, Iacovoni JS, Álvarez-Quilón A, Cortés-Ledesma F, Legube G. 2015. Non-redundant functions of ATM and DNA-PKcs in response to DNA double-strand breaks. Cell Rep 13:1598–1609. https://doi.org/10.1016/j.celrep.2015.10.024.
47. Aymard F, Aguirrebengoa M, Guillou E, Javierre BM, Bugler B, Arnould C, Rocher V, Iacovoni JS, Biernacka A, Skrzypczak M, Ginalski K, Rowicka M, Fraser P, Legube G. 2017. Genome-wide mapping of long-range contacts unveils clustering of DNA double-strand breaks at damaged active genes. Nat Struct Mol Biol 24:353–361. https://doi.org/10.1038/nsmb.3387.
48. Koike-Yusa H, Li Y, Tan E-P, Velasco-Herrera MDC, Yusa K. 2014. Genome-wide recessive genetic screening in mammalian cells with a lentiviral CRISPR-guide RNA library. Nat Biotechnol 32:267–273. https://doi.org/10.1038/nbt.2800.
49. Hsu PD, Scott DA, Weinstein JA, Ran FA, Konermann S, Agarwala V, Li Y, Fine EJ, Wu X, Shalem O, Cradick TJ, Marraffini LA, Bao G, Zhang F. 2013. DNA targeting specificity of RNA-guided Cas9 nucleases. Nat Biotechnol 31:827–832. https://doi.org/10.1038/nbt.2647.
50. Dorsett Y, Zhou Y, Tubbs AT, Chen B-R, Purman C, Lee B-S, George R, Bredemeyer AL, Zhao J, Sodergen E, Weinstock GM, Han ND, Reyes A, Oltz EM, Dorsett D, Misulovin Z, Payton JE, Sleckman BP. 2014. HCoDES reveals chromosomal DNA end structures with single-nucleotide resolution. Mol Cell 56:808–818. https://doi.org/10.1016/j.molcel.2014.10.024.
51. Chicaybam L, Barcelos C, Peixoto B, Carneiro M, Limia CG, Redondo P, Lira C, Paraguassú-Braga F, De Vasconcelos ZFM, Barros L, Bonamino MH. 2016. An efficient electroporation protocol for the genetic modification of mammalian cells. Front Bioeng Biotechnol 4:99. https://doi.org/10.3389/fbioe.2016.00099.
52. Collins PL, Kyle KE, Egawa T, Shinkai Y, Oltz EM. 2015. The histone methyltransferase SETDB1 represses endogenous and exogenous retroviruses in B lymphocytes. Proc Natl Acad Sci U S A 112:8367–8372. https://doi.org/10.1073/pnas.1422187112.
53. Collins PL, Cella M, Porter SI, Li S, Gurewitz GL, Hong HS, Johnson RP, Oltz EM, Colonna M. 2019. Gene regulatory programs conferring phenotypic identities to human NK cells. Cell 176:348–360.e12. https://doi.org/10.1016/j.cell.2018.11.045.
54. Ramírez F, Ryan DP, Grüning B, Bhardwaj V, Kilpert F, Richter AS, Heyne S, Dündar F, Manke T. 2016. deepTools2: a next generation web server for deep-sequencing data analysis. Nucleic Acids Res 44:W160–W165. https://doi.org/10.1093/nar/gkw257.
55. Karolchik D, Baertsch R, Diekhans M, Furey TS, Hinrichs A, Lu YT, Roskin KM, Schwartz M, Sugnet CW, Thomas DJ, Weber RJ, Haussler D, Kent WJ, University of California Santa Cruz. 2003. The UCSC Genome Browser Database. Nucleic Acids Res 31:51–54. https://doi.org/10.1093/nar/gkg129.
56. Langmead B, Salzberg SL. 2012. Fast gapped-read alignment with Bowtie 2. Nat Methods 9:357–359. https://doi.org/10.1038/nmeth.1923.
57. Quinlan AR, Hall IM. 2010. BEDTools: a flexible suite of utilities for comparing genomic features. Bioinformatics 26:841–842. https://doi.org/10.1093/bioinformatics/btq033.
58. Love MI, Huber W, Anders S. 2014. Moderated estimation of fold change and dispersion for RNA-seq data with DESeq2. Genome Biol 15:550. https://doi.org/10.1186/s13059-014-0550-8.
59. Hung PJ, Johnson B, Chen B-R, Byrum AK, Bredemeyer AL, Yewdell WT, Johnson TE, Lee BJ, Deivasigamani S, Hindi I, Amatya P, Gross ML, Paull TT, Pisapia DJ, Chaudhuri J, Petrini JJH, Mosammaparast N, Amarasinghe GK, Zha S, Tyler JK, Sleckman BP. 2018. MRI is a DNA damage response adaptor during classical non-homologous end joining. Mol Cell 71:332–342.e8. https://doi.org/10.1016/j.molcel.2018.06.018.